



Acoustofluidic closed-loop control of microparticles and cells using standing surface acoustic waves

Tan Dai Nguyen^a, Yong Qing Fu^b, Van-Thai Tran^a, Archana Gautam^a, Sanam Pudasaini^a, Hejun Du^{a,*}

^a School of Mechanical and Aerospace Engineering, Nanyang Technological University, 639798, Singapore

^b Faculty of Engineering and Environment, Northumbria University, Newcastle upon Tyne, NE1 8ST, UK

ARTICLE INFO

Keywords:

Microfluidics
Lab-on-a-chip
Acoustofluidics
Surface acoustic waves
Closed loop control

ABSTRACT

Precise, automatic and reliable position control of micro-objects such as single particles, biological cells or bio-organisms is critical for applications in biotechnology and tissue engineering. However, conventional acoustofluidic techniques generally lack reliability and automation capability thus are often incapable of building an efficient and automated system where the biological cells need to be precisely manipulated in three dimensions (3D). To overcome these limitations, we developed an acoustofluidic closed-loop control system which is combined with computer vision techniques and standing surface acoustic waves (SSAWs) to implement selective, automatic and precise position control of an object, such as a single cell or microparticle in a microfluidic chamber. Position of the object is *in situ* extracted from living images that are captured from a video camera. By utilizing the closed-loop control strategy, the object is precisely moved to the desired location in 3D patterns or along designed trajectories by manipulating the phase angle and power signal of the SSAWs. Controlling of breast cancer cells has been conducted to verify the principle and biocompatibility of the control system. This system could be employed to build an automatic system for cell analysis, cell isolation, self-assembling of materials into complex microstructures, or lab-on-chip and organ-on-chip applications.

1. Introduction

Precise, automatic and reliable control of single cells is essential in biotechnology and tissue engineering for tasks of cell sorting and manipulation [1–6], cell analysis and screening [1,5,7–9], cell isolation [8,10], self-assembly of cells and tissues [11–15]. The common technique using optical tweezers [16,17] could achieve a high precision but usually face the problems of relatively weak forces and highly intense power that causes the damage to the living cells [18]. In the past decades, surface acoustic waves (SAWs) have been extensively studied and considered as a powerful tool to replace the optical tweezer for applications in microfluidics and biomedical engineering due to the noninvasive, biocompatible, label-free, low-power consumption and inexpensive technique [19–21]. SAWs are generated by the propagation of mechanical waves on surface of elastic materials, and these waves have been applied to control the fluid and particles inside the fluid for numerous microfluidic applications [19,20,22]. The acoustic tweezers created from the standing SAWs (SSAWs) have been used to precisely trap, transport and manipulate objects within the 2D plane by either modulating the operating frequency or shifting the relative phases of

resonant-frequency signals generated from the two opposite inter-digital transducers (IDTs) [18,23–25]. For manipulating purposes, the phase shifting method has more advantages than frequency sweeping, such as better flexibility and larger working range [26]. In term of single-cell manipulation, SSAWs are able to trap a wide range of the cells with different sizes, shapes, densities and compressibility properties [19].

The current manipulation techniques based on SSAWs are mostly using open-loop control strategy which delivers the output manipulation (e.g. shifting the phase or modulating the frequency) independent of the motions of the manipulating objects, (e.g. particle, bubble and cell). These systems have been applied in the fields of microfluidics, especially the manipulation of micro/nanoparticles, microbubbles, cells, molecules to generate multiple functions of focusing [27–29], manipulating [30,31], separating [32–42], isolating [10,43], patterning [24,44–46] and positioning [2,3,47]. SSAWs have extensively been used to control rotation and transportation of single cells in the past few years [5,10,18,23,44,48–54]. However, the general open-loop control systems face significant challenges, such as unreliability and time-consuming process due to manual control and no detailed information

* Corresponding author.

E-mail address: MHDU@ntu.edu.sg (H. Du).

<https://doi.org/10.1016/j.snb.2020.128143>

Received 28 November 2019; Received in revised form 24 February 2020; Accepted 14 April 2020

Available online 25 April 2020

0925-4005/ © 2020 Elsevier B.V. All rights reserved.

for changes of object's positions. For example, they cannot recognize the unexpected motions of objects caused by noise or external vibrations. Therefore, it is critically demanded for a system to monitor these changes and efficiently adjust object's positions. To solve this problem, a closed-loop control strategy could be implemented to extract the exact position of the objects and precisely adjust their movement. The closed-loop control strategy has been applied in microfluidic system to control the volume of droplet and fluid-height in open reservoirs over recent years [55–58]. However, to the best of our knowledge, there is no any previous report for using close-loop control systems for acoustofluidic devices.

In this study, we proposed the integration of a control system into an acoustofluidic device in order to improve the controlling efficiency of cells or microparticles in 3D space using the SSAWs. A computer vision algorithm was employed to detect the current positions of the object from the captured image, which serves as a feedback signal. Based on the feedback, a closed-loop controller then transmits the manipulation signal to adjust position of the particle by shifting the relative phase angles of the frequency signals generated by the opposite IDTs for in-plane motion (x - y coordinates), or adjusting the SAW power for out-of-plane motion (z coordinate). It is worthwhile to note that the integration of closed-loop control strategy technically would not improve the resolution of the SAW device, for example, the resolution of phase-shifting method still depends on the phase division of equipment resolution. The characteristics of the closed-loop control system tested on polystyrene microparticles such as speed, resolution and response time were investigated. Thereby, a microparticle with diameter of $20\ \mu\text{m}$ was separated from the $10\ \mu\text{m}$ microparticles at the speed limit. Automatic control of single microparticle to one location and to follow a 2D arbitrary trajectory was performed. Combination of in-plane and out-of-plane control system was performed to demonstrate the 3D controlling capability. Breast cancer cells (MCF-7) were used to test the principle and compatibility of the control system for biological applications.

2. Method

2.1. Device fabrication

Fig. 1(a) shows an optical image of the assembled SAW system, and Fig. 1(b) shows the working area inside the chamber. The piezoelectric substrate is 128° Y-cut lithium niobate (LiNbO_3). The IDTs were patterned using the standard photolithography followed by a lift-off process to obtain metal electrodes (Cr/Au, 10 nm/50 nm) on the LiNbO_3 wafer. The IDTs have 60 pairs of fingers with both width and space gap of $75\ \mu\text{m}$, corresponding to a SAW wavelength of $300\ \mu\text{m}$ and an aperture of 1 cm. A cubic polydimethylsiloxane (PDMS) chamber (Sylgard 184 Silicone Elastomer; Dow Corning, USA) was aligned with the

IDT patterns to ensure the forming lines of trapped objects are parallel to the IDT fingers and bonded on top of the piezoelectric substrate after being treated with oxygen plasma. The chamber is 1.5 mm wide (covering five SAW wavelengths), $100\ \mu\text{m}$ tall for 2D manipulation or $1000\ \mu\text{m}$ for 3D manipulation, and it was prepared using a soft casting method and a mold made using a computer numerical controlled (CNC) machine.

2.2. Cell preparation

Michigan Cancer Foundation-7 (MCF-7) breast cancer cell line, purchased from the American Type Culture Collection, were cultured in Dulbecco's Modified Eagle Medium (Gibco; Thermo Fisher Scientific, USA) supplemented with 10 % FBS and 5 % antibiotic. The cells were maintained to grow in a humidified environment at 37°C and 5 % CO_2 for three to four days until 70–80 % confluence was reached. After that, they were trypsinized with 0.05 % trypsin and collected by centrifuging at 250 g for 5 minutes. The cell pellet was re-suspended in the media and counted by hemocytometer.

2.3. System setup

To record the microparticle or cell images, a charge-coupled device (CCD) camera (DFK 51BG02.H; IVS Imaging, USA) was connected to an optical microscope (M150 Probe Station; Cascade Microtech, USA). The controller program was written in MATLAB R2018b (MathWorks, USA) embedded in the laptop (Ideapad 310; Lenovo, China). The controller was connected to the camera to acquire the live images and the signal generators (MHS-5200 P; Ming Wo Electronics, China) to send the manipulating signal (Fig. 2). The signal was then amplified by an RF amplifier (the amplifier characteristics are provided in Fig. S1) before being applied to the IDTs to generate the SSAWs. The resonant frequency was measured using an impedance analyzer (4294A Impedance Analyzer; Agilent, USA). We performed frequency-sweep measurements to scan a wide frequency range, and the resonant frequency was obtained at its highest impedance. The resonant frequencies for the IDT pairs along two orthogonal directions were measured to be 13.193 MHz and 12.124 MHz, due to the isotropically piezoelectric property of LiNbO_3 substrate. The microparticles of two different sizes (polystyrene microspheres with average diameters of $10\ \mu\text{m}$ and $20\ \mu\text{m}$; Polysciences, USA) and MCF-7 cells were injected into the chamber using a pipette.

2.4. Working principle

When the SAW device is operated at its resonant frequency, the waves generated from the two identical but opposite IDTs will propagate on the substrate and interact with the fluid to form the leaky SAWs

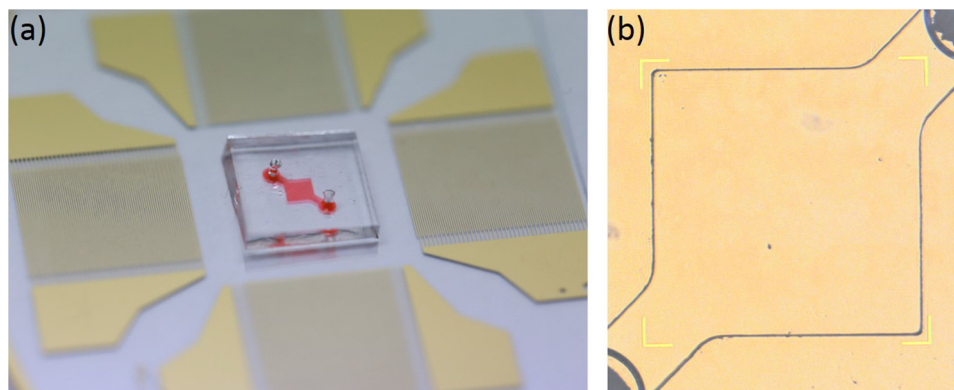


Fig. 1. (a) An optical image of the device after fabrication including interdigital transducers (IDTs), polydimethylsiloxane (PDMS) chamber, inlet and outlet. (b) The aligned PDMS chamber filled with DI water.

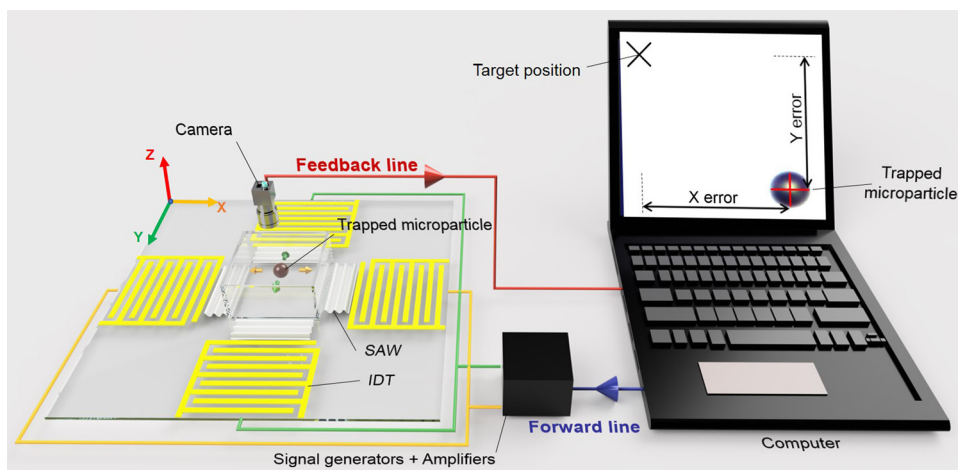


Fig. 2. Illustration of closed-loop control system operation. A computer is connected to a camera to track the microparticle's position on feedback line and a SAW device through signal generators and amplifiers (the black box) on forward line. The trapped microparticle can move along x and y directions by shifting the relative phase of signal from opposite IDTs or z direction by turning the power. The computer's monitor shows a tracked microparticle was marked by the red "+" sign and the target position is marked by the black "x" sign.

and also create the SSAWs [59]. A pressure gradient is generated inside the liquid, forming pressure nodes (minimum pressure amplitude) and anti-pressure nodes (maximum pressure amplitude). The suspended objects in fluid are subjected to the combined forces: e.g., (1) the acoustic radiation force generated from the pressure fluctuations; (2) the Stoke drag force caused by the acoustic streaming which arises from the nonlinear propagation of a SAW through an attenuating media [60]; (3) gravity force; and (4) buoyant force. The acoustic radiation force is given by [61]:

$$F_{\text{rad}} = -\nabla \left\{ V_p \left[\frac{f_1}{2\rho_0 c^2} \langle p_1^2 \rangle - \frac{3\rho_0 f_2}{4} \langle u_1 \cdot u_1 \rangle \right] \right\} \quad (1)$$

where

$$f_1 = 1 - \frac{\rho_0 c^2}{\rho_p c_p^2} \quad (1a)$$

$$f_2 = \frac{2(\rho_p - \rho_0)}{2\rho_p + \rho_0} \quad (1b)$$

in which u_1 is the first-order velocity, p_1 is the first-order pressure, V_p is the volume of spherical object, ρ_p and c_p are density and speed of sound of object, respectively. As we are considering a quiescent liquid (e.g., water) before the presence of any acoustic wave, the initial pressure and density are assumed as constants, i.e., p_0 =static pressure, ρ_0 =998kg/m³.

The Stoke drag force is given by [62]:

$$F_{\text{d}} = 6\pi\mu R(\langle v_2 \rangle - v_p) \quad (2)$$

where R is the radius of the object, v_p is the object velocity and v_2 is the second order velocity or acoustic streaming velocity.

From Eq.s (1) and (2), the acoustic radiation force is proportional to the volume (R^3) of the object while the drag force is proportional to the radius (R) of object. Therefore, the larger size object are experienced with the larger acoustic radiation force, thus they move much faster to either the pressure nodes or anti-pressure nodes, depending on the relative density and compressibility of object to medium [63]. In our experiment, we used the polystyrene beads in the DI water and the MCF-7 cells in cultured medium, which move towards the pressure nodes when experience the acoustic radiation force.

As the objects are trapped at the acoustic pressure nodes or acoustic tweezers, the in-plane movement of objects is realized by tuning acoustic tweezer's position. This is achieved by simply shifting the signal phase-angle of opposite IDTs. If the chamber is high enough (e.g., 1 mm), 3D aligned patterns with multilayers of 3D acoustic tweezers along the height (or vertical) direction are generated due to the reflection of acoustic waves from substrate to the top of chamber [45,49].

The interlayer distances are identical and determined by f/c , where f is the operating frequency and c is speed of sound in fluid. The object could be trapped into these 3D acoustic tweezers or levitated/dropped by manipulating the SAW signal power.

The setup and operation of the in-plane closed-loop control system on a microparticle are illustrated in Fig. 2. It includes a controller (i.e., a computer's algorithm written in MATLAB code), which is connected to a camera (on the feedback line) and the SAW device through signal generators and amplifiers (on the forward line). The computer's monitor shows the selected single microparticle after being trapped into an acoustic tweezer (marked with the red "+" sign) and the target position (marked with the black "x" sign). The distances between the microparticle and the target position along both the x and y directions are called the distance errors. The objective of using the closed-loop controller is to minimize these errors (including x error and y error) to effectively manipulate the microparticle to the target position. In operation, the controller initially detects the current position of the microparticle from the optical image, which is *in-situ* captured by microscope's camera, using a computer vision algorithm on the feedback line. This algorithm relies on the contrast between black microparticle and the white background, the "regionprops" command in MATLAB is applied to determine the centroid's position of microparticle. The distance error between the target position and the microparticle's position is then calculated. As the response, the controller will change (either increase or decrease) the relative phase angles of the radio-frequency signal on the forward line to relocate microparticle's position so that the distance error is minimized. The loop operates in the real time and will be paused when the distance errors in both x and y directions are smaller than a constant tolerant value, which means that the microparticle has reached the target position. The purpose of using a constant tolerant value of 5 pixels is to shorten the matching process. At this time, the controller will load the next target position and repeat the loop process until the microparticle reaches the targeted positions. The flowchart of algorithm and the block diagram are presented in Figs. S2 and S4, respectively, in the SI document.

3. Results and discussion

3.1. Response time, speed measurement and separation of different-sized microparticles

We firstly evaluated the closed-loop control system by investigating the dynamic response a single microparticle, as a function of time. Fig. 3(a) and (b) show the obtained displacement response curves of a single microparticle with a diameter of 10 μm along x and y directions, respectively. On each direction, the microparticle took around 30 s to reach the target position over the distance of 500 pixels. It should be

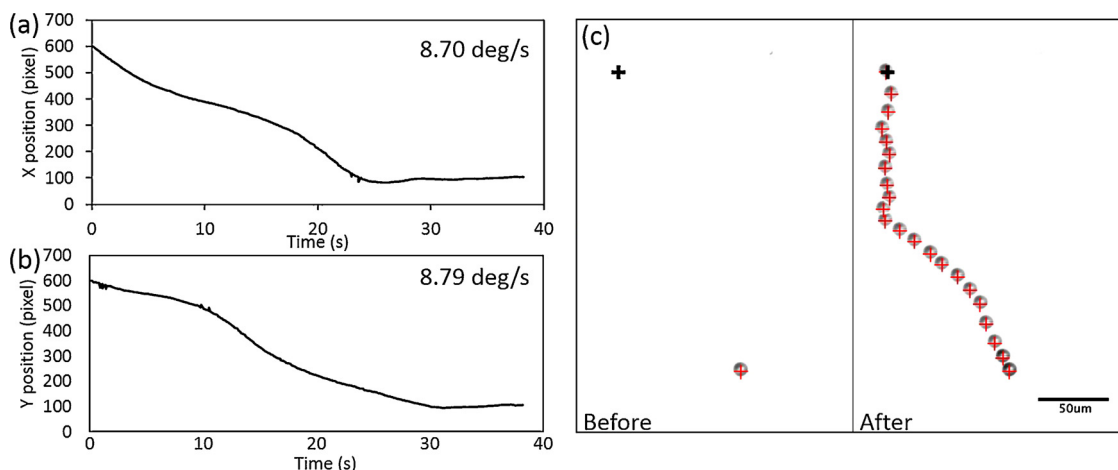


Fig. 3. (a) and (b) Response times of a single microparticle with a 10 μm diameter after being controlled to move from 600 to 100 pixels position with the phase-shifting speeds are 8.7 deg/s and 8.79 deg/s along x and y directions, respectively. (c) The stacked images of microparticle's position before and after being controlled simultaneously both x and y directions to move to the target position which is the black "+" sign on the left corner.

noted that the distance of 1 μm along x direction corresponds to 1.8 pixels, whereas along y direction it corresponds to 2.1 pixels. Fig. 3(c) shows the stacked image of the same microparticle before and after applying the closed-loop control, simultaneously, on both x and y directions to relocate it to a 2D target position (the black plus sign on the left corner) over the distance of 980 pixels. The response time is strongly dependent on phase-shifting speed. The linear relationship between the phase change and displacement has been reported previously in literature [64]:

$$\Delta d = (n-1) \frac{\lambda}{2} + \frac{\lambda}{720^\circ} \varphi \in [0^\circ, 360^\circ] \quad (3)$$

where Δd is the displacement, $n = 1, 2, 3, \dots$ represents the number of the repetition of changing the relative phase from 0° to 360° ; φ is the relative phase opposite IDTs; λ is the wavelength of the SAW.

The in-plane resolution of the SAW device is defined as the minimum distance of object movement or the smallest increment of displacement that the device can achieve. Since our signal generator has resolution of 1 degree and the SAW device has the designed wavelength of 300 μm , hence, the theoretical minimum displacement for shifting the phase for 1 degree is calculated to be $\sim 0.42 \mu\text{m}$ (i.e., $300 \mu\text{m} \times 1 \text{ degree}/720 \text{ degree}$) based on Eq. (3). In our experiments, it is challenging to detect this tiny displacement of microparticles by using a standard video camera. Instead, we recorded the transportation distance of a single microparticle with a diameter of 10 μm after the phase angle was shifted for 20 degrees. Results showed that the microparticle was moved ~ 15 pixels in both x and y directions. However, it should be addressed that the pixel's sizes are slightly different in two directions, which is defined as the pixel aspect ratio of camera sensor. The dimensions of a single pixel along x and y directions are 2.1 pixels/ μm and 1.8 pixels/ μm , respectively. Accordingly, the in-plane resolution of the SAW device was calculated to be $\sim 0.36 \mu\text{m}/\text{deg}$ along the x direction and $\sim 0.42 \mu\text{m}/\text{deg}$ along the y direction which approximately similar to the theoretical value. It is worthwhile to note that the resolution of the SAW device does not reflect the resolution of the control system. The resolution of a control system is defined as the smallest movement of microparticle that can be detected by the camera. In our control system, it is equal to the size of one pixel which is $\sim 0.48 \mu\text{m}/\text{pixel}$ along x direction and $\sim 0.56 \mu\text{m}/\text{pixel}$ along y direction. Based on this, using a higher resolution camera paves a way to build a higher resolution control system. With SAW devices operated at a higher frequency or with a smaller wavelength, their resolution could be further improved. For example, for a SAW device which has a wavelength of 0.8 μm [65], the corresponding resolution is calculated to be $\sim 1.1 \text{ nm}$ (i.e., $0.8/720$). However, it might then become time-consuming and

impractical to control over a large distance at a very high resolution. This can be resolved by integrating multiple wavelengths into a single IDT [66]. Whereby, the low-resolution manipulation (i.e., using devices with larger wavelengths or smaller frequencies) can be used for a rough adjustment of movement while the high-resolution manipulation (i.e., using devices with smaller wavelengths or higher frequencies) for a fine adjustment of precise movement.

Generally, the increase of phase-shifting speed leads to a higher velocity of the microparticle. In our experiment, we investigated the relation between phase-shifting speed and microparticle's velocity along x direction. Fig. 4(a) shows that the changes of the microparticle's velocity has a linear relationship with the phase-shifting speed. With an increase of phase-shifting speed (equal to or larger than a limit of 30 deg/s), we found that the microparticles could be extricated from the trapping acoustic tweezer (Fig. 4(a)). This can be explained that while the acoustic radiation force pushes the microparticle to follow the moving acoustic tweezer, but the drag force caused by the motion of microparticle in the fluid as described by equation (2) has the opposite direction to pull the microparticle out of acoustic tweezer. The higher the microparticle's speed, the stronger the drag force is and thus the easier for the particles to be extricated. However, because the SSAWs have created an acoustic tweezer pattern with equal intervals [24], after extricated from one acoustic tweezer, the microparticle will be trapped to the next acoustic tweezer. As a result, this phenomenon causes the microparticle to oscillate back and forth (e.g., trapped then released). A video recorded for this phenomenon is shown in the **SI-video 1**.

Based on the Eq. (1), there are three ways which we can increase the speed limit through increasing the amplitude of acoustic radiation force, in the other words, increasing the trapping strength of acoustic tweezer. (i) Firstly, increasing the operating power in order to increase the first-order acoustic pressure. However, applying a higher power will induce more heat inside the chamber [67]. The results of temperature change of fluid inside microchamber for 10 minutes are presented in Fig. S3 of **SI document**. Our results suggested that the generated heat can be minimized by integrating a Peltier cooler beneath the SAW device; (ii) Secondly, using larger size microparticles or gathering small microparticles into a large group and (iii) Finally, increasing operating frequency, which will strengthen the acoustic radiation force [44].

In fact, the acoustic radiation forces generated from the acoustic pressure field are strongly dependent on the size of microparticles [61,68]. Various microfluidic devices have relied on this principle to continuously separate or sort the microparticles or cells from different sizes and densities [10,34,36–39,41,69]. Herein, we took advantage of

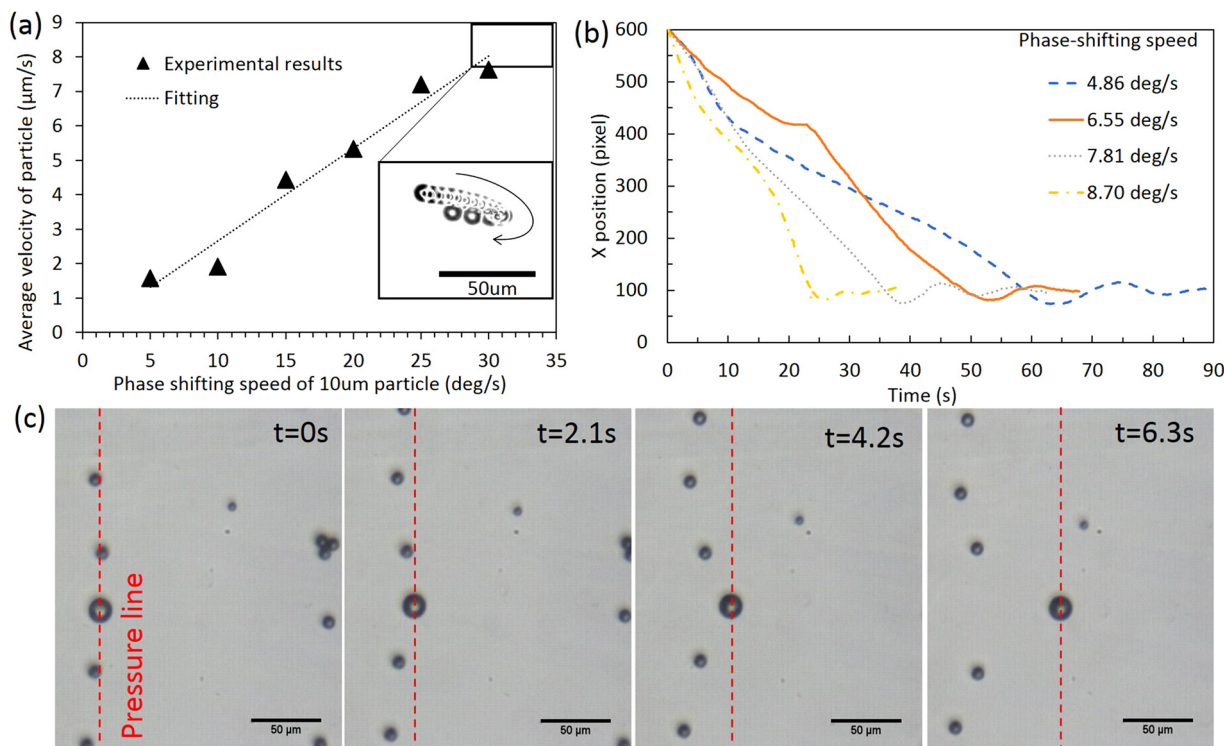


Fig. 4. (a) The relationship between microparticle's velocity and phase-shifting speed. At shifting speed higher than 30 deg/s, the microparticle will be extricated from acoustic tweezer and oscillated back and forth. (b) The response time of 10 μm diameter microparticle moved from position 600 pixels to 100 pixels at different phase-shifting speeds along x direction. (c) Controlling the 20 μm and 10 μm diameter microparticles to the right direction at the speed of 30 degrees/s. Before controlling, all microparticle trapped and aligned along vertical red line. After controlling, 20 μm diameter microparticle was separated from 10 μm diameter microparticles (scale bar: 50 μm).

above extrication phenomenon to separate different-sized microparticles. Two sizes of polystyrene microparticles with diameters of 10 μm and 20 μm were used for this investigation. At the initial stage, all of microparticle were trapped into an acoustic tweezer and aligned to the same vertical line (as shown in the red dash in Fig. 4(c)) after the power was turned on to the horizontal pair of IDTs at a power of 28.5 dBm. Then, the relative phase was shifted at a speed of 30 deg/s rightward. The result in Fig. 4(c) shows that the 10 μm microparticles were extricated from the acoustic tweezer whereas the 20 μm microparticles were still trapped and moved. This is because the 20 μm microparticles experienced a larger (~ 8 times based on Eq. (1)) acoustic radiation force than the 10 μm microparticles, and thus are able to follow the shifting acoustic tweezers while the 10 μm microparticles were extricated. This phenomenon is useful for isolation and separation applications such as separating a specific cell [43].

We have further measured the response time with the increase of phase-shifting speed at a given power of 28.5 dBm. The results in Fig. 4(b) show the response time for the microparticle to reach the desired position of 100 pixels is inversely proportional to phase-shifting speed. The shorter the response time, the faster the microparticle moves to the desire location, which generally increases the efficiency of the system.

3.2. Demonstration of 2D, 3D and biological cell manipulation

In this section, we applied the closed-loop system to control a single microparticle in a designed arbitrary trajectory to draw a letter of "NTU". This is achieved by setting a chain of target positions in the shape of the "NTU" letters written using AutoCAD software as shown in Fig. 5(a). Fig. 5(d) shows how a tracked microparticle approaches and arrives to a target point in the dash line boxes and then continue to move to another target point in the continued line boxes. It should be pointed out that the target position will be changed to the new value

when the distance errors are smaller than 5 pixels. Fig. 5(b) shows the experimental trajectory of the microparticle. Each point in this trajectory was the captured position of the microparticle. Fig. 5(c) shows a combined image by stacking multiple images of microparticle at different moments. A recorded video of the whole process is presented in the SI-video 2.

In Fig. 5(b), the trajectory of the microparticle are not smooth at some points. This is caused by the external vibrations from ground or equipment and also from the effect of the acoustic streaming that leads to the extrication of microparticle from acoustic tweezer. However, the closed-loop system can regulate the microparticle back to the desired path afterward. To eliminate the external noise, the whole experimental system is recommended to be set on an anti-vibration table. Additionally, an advanced controller such as artificial intelligent algorithm will further improve the performance of the controlling system [70]. The acoustic streaming dominates the motion of microparticles when their sizes are below the frequency-dependent critical crossover size, and vice versa, the acoustic radiation force becomes dominant again [5,71]. In order to reduce the effect of acoustic streaming, the microparticle's size is needed to be above their critical size, otherwise, the device needs to be redesigned at a higher operating frequency. Due to the automatic and precise control of microparticle, this method could be employed to couple with the lab-on-chip and organ-on-chip device for precise transportation purposes. This could assist the studies of cell such as cell-cell interaction and communication by controlling the distance of cells or fixing the position of the single cell for analysis or transfection [2].

3D assembly using programmable system in combination with acoustic tweezer has seldom been reported. In addition to the manipulation in the x-y coordinates (in-plane), the manipulation along z coordinate (out-of-plane) has been achieved by turning the power applied to SAW device [18,45]. In the 3D chamber, the SSAWs generate multiple and periodic trapping layers along z direction [45]. On each

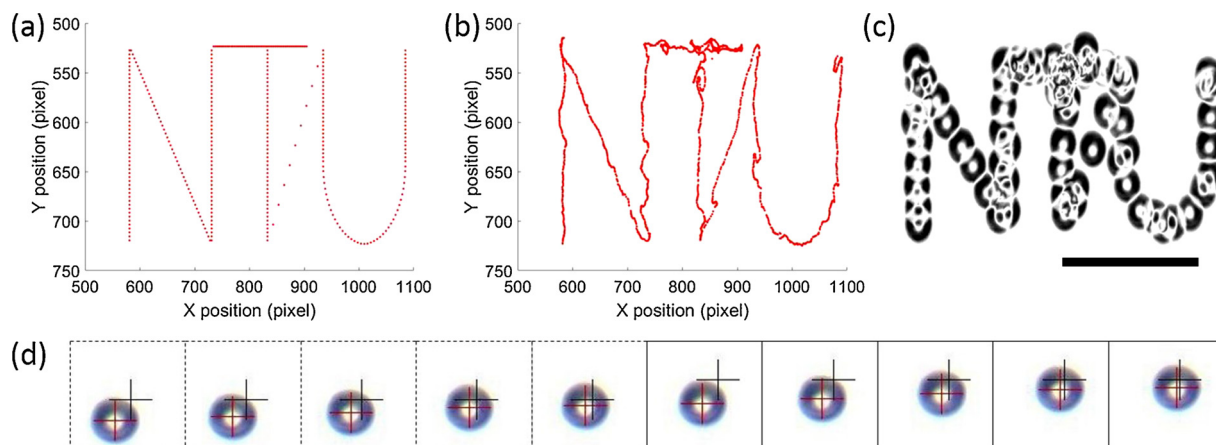


Fig. 5. Manipulation of 10 μm diameter single microparticle to write a “NTU” letter. (a) The “NTU” letter which are point series designed using AUTOCAD software. (b) The recorded trajectory of microparticle during the continuous manipulation. (c) The stacked images of microparticle at different moments to show the word of “NTU” (scale bar: 50 μm). (d) The approaching of the microparticle to the first (dash line boxes) and second (continued line boxes) target point.

layer, the acoustic radiation force is directed to trapping nodes. After trapping, the microparticles can be either levitated to upper layers by turning on the power of SAW device; or dropped down to lower layers by switching off the SAW power. Basically, turning on the SAW power will increase the difference between upward and downward acoustic radiation forces applied to the microparticle and thus result in a stronger upward net force. This force levitates the microparticle to the higher layer. Afterward, the microparticle can be locked into that new layer by returning the power to the previous value. The dropping of the particle occurs after switching off the power because of the gravity, which is strongly dependent on the weight of microparticle.

In terms of controlling range, the manipulation is capable of operating in the whole range of 1 mm height of the chamber. For example, a high power will raise the microparticles to the top surface of the chamber. In term of vertical resolution of the SAW device, the inter-layer distance of layers defines the resolution along z direction. In our experiment, this distance is approximated about 60 μm and could be reduced by changing to the device with higher operating frequency. In terms of time scale, the raising-up of particle could be quickly achieved but the dropping may be time consuming. Therefore, the heavier microparticles not only accelerate the process but also reduce the effect of the acoustic streaming, thus facilitating the efficient controlling process. The smaller and lighter microparticles become heavier when forming into groups with the aid of SSAWs aggregation [24]. Herein, we combined the out-of-plane control technique with the in-plane

control technique to enable the three-dimensional manipulation capability. A demonstration in Fig. 6(a) shows the side-view of 20 μm diameter microparticle at different moments moved along a rectangular shape. The prism was applied to enable the horizontal view as mentioned in our previous study [45]. Initially, the microparticle was fixed at its initial position when turning on the power of 27.1 dBm (point A). After that, it was levitated over a distance of 178 μm by increasing the power to 33.4 dBm and then returning to 27.1 dBm immediately to fix the microparticle to the new position (point B). Phase-shifting was then applied to move the microparticle to the left over a distance of 133 μm (point C). The power was subsequently turned off to drop the microparticle and turned on again when it reached the same height as the beginning point (point D). Finally, we shifted the phase in the opposite direction to bring it back to the original position (point A). A recorded video of this process can be found in the **SI-video 3**. In this recorded video, it is easy to realize that the microparticle was stopped at different layers when levitating from point A to point B.

In order to integrate the out-of-plane control into the same closed-loop system with the in-plane control system, we propose to apply the focus function of the microscope to provide a feedback for the vertical position of the microparticle. Prior to applying the control, the targeted height position of microparticle relative to the bottom surface of chamber needs to be determined based on the height of multilayers of 3D pattern where the microparticles are capable to be trapped. Subsequently, the microscope is focused at the substrate’s surface and

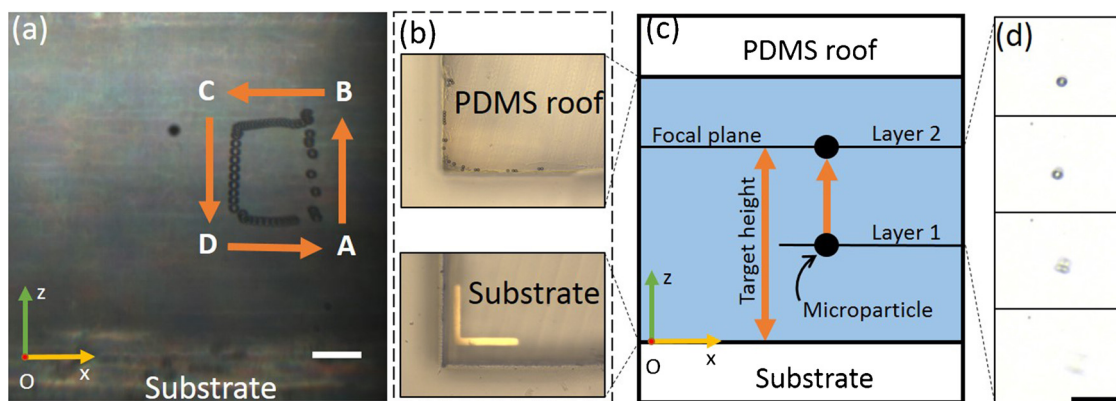


Fig. 6. (a) The stacked images of 20 μm diameter microparticle at different moments moved along a rectangular shape which observed from the side view. The arrows show the moving direction. (b) Experimental vertical view of the chamber’s top surface or PDMS roof and the chamber’s bottom surface or substrate. (c) Diagram describe the set-up of target height same as the focal plane and the lifting of microparticle from layer 1 to layer 2 by increasing the power. (d) The experimental result of lifting microparticle with diameter of 10 μm from unfocused to be focused (bottom to top images) at focal plane (scale bar: 50 μm).

the exact position of focus knob is recorded as a reference's value (Fig. 6(b)). Then, we turn the focus knob to the new value which the subtraction from the reference's value is equal to the target height (layer 2 in Fig. 6(c)). As long as the focal plane match the target height position, the microparticle will be levitated/dropped until its image under microscope is sharpest or in-focus. This means that the vertical position of microparticle has reached to the targeted height position. A demonstration is shown in Fig. 6(d), in which we turned the power to lift a microparticle with diameter of 10 μm from the unfocused position to the focused position in a 1 mm-height chamber at the height of 780 μm (about 12th layer from the bottom surface). The block diagram of this out-of-plane control system has been presented in Fig. S5 in the **SI document**. A combination of x–y and z closed-loop control results in a three-dimensional closed-loop control system. The object could be controlled in the x–y coordinates and then along the z coordinate, or vice versa. In tissue engineering, this is a promising technique to build up a micro-bio-system for assembling of 3D complex constructs of biomaterials.

The application of SAWs for biological cells has been extensively studied in the literature [18,23,24,44,51–53,66,69,72,73]. To verify the compatibility of the closed-loop control system with biological cells, we performed the closed-loop control of single breast cancer cell (MCF-7) from a random position to the targeted position at the coordinate (x, y) = (100, 100) pixels. The cell was kept in its original medium with added Trypan Blue stain (0.4 %, Life Technologies, USA) for the viability test. Fig. 7(a) shows the stacked images of the tracked cell at different durations. The random shape and rotation of the cell during its moving caused difficulty for the computer vision algorithm to detect the centroid position of the cell. Although there are apparent noises as shown in Fig. 7(b), it was still in a good control pattern because of the high contrast between the cell and background. Moreover, we can extract the real movement of the cell from the recorded trajectory as shown in the zoomed image in Fig. 7(b). A digital filter is recommended to integrate into the computer algorithm, in order to eliminate most of these noises. The cell was still alive after manipulation as it did not take up the dye. A recorded video of this process can be found in the **SI-video 4**.

In addition, as the cell would rather attach the others and thus form groups, therefore, we have exploited the closed-loop system to control a group of cells. Fig. 7(c) shows the result of a group of MCF-7 cells before and after being relocated to the target position at (100, 100) pixels. In this case, the algorithm was defined to detect many cells at once which could confuse the controller about the current position of the cell. However, our results showed that as long as the distance errors are still existed, the controller kept shifting the relative phase in order to minimize the distance errors. As a result, the group of cell was relocated to the targeted position at (100, 100) pixels. A recorded video of this

process can be found in the **SI-video 5**.

4. Conclusion

In conclusion, by integrating a closed-loop control strategy with the acoustic tweezer, our acoustofluidic closed-loop system paves the way for controlling microparticle or cell in an effective manner. A single microparticle is able to follow any desired trajectory automatically in a 3D pattern by the automatic manipulation of relative phases and power of the SAW device. The characteristics of the closed-loop control system have been investigated. Notably, the speed limit of shifting acoustic tweezers was explored to use in order to separate the larger size objects, which is suitable for isolation and separation applications. Controlling of a single and a group of breast cancer cells have been conducted to verify the principle and biocompatibility of the control system. This acoustofluidic closed-loop control system serves as an effective tool to develop an automatic process for cell-cell interaction, cell analysis, cell manipulation as well as self-assembling of materials into complex microstructures. The aid of computer vision in the closed-loop system is also useful to collect the cell images for screening studies.

CRediT authorship contribution statement

Tan Dai Nguyen: Conceptualization, Data curation, Software, Methodology, Formal analysis, Investigation, Visualization, Writing - original draft, Writing - review & editing. **Yong Qing Fu:** Conceptualization, Funding acquisition, Project administration, Supervision, Writing - review & editing. **Van-Thai Tran:** Conceptualization, Investigation, Writing - review & editing. **Archana Gautam:** Investigation, Resources. **Sanam Pudasaini:** Investigation, Resources. **Hejun Du:** Conceptualization, Funding acquisition, Resources, Methodology, Project administration, Supervision, Validation.

Declaration of Competing Interest

The authors declare that they have no known competing financial interests or personal relationship that could have appeared to influence the work reported in this paper.

Acknowledgments

The authors gratefully acknowledge the support of (i) Nanyang Technological University and the Ministry of Education of Singapore through a PhD Scholarship; (ii) the UK Engineering and Physical Sciences Research Council (EPSRC) grants EP/P018998/1; (iii) Special

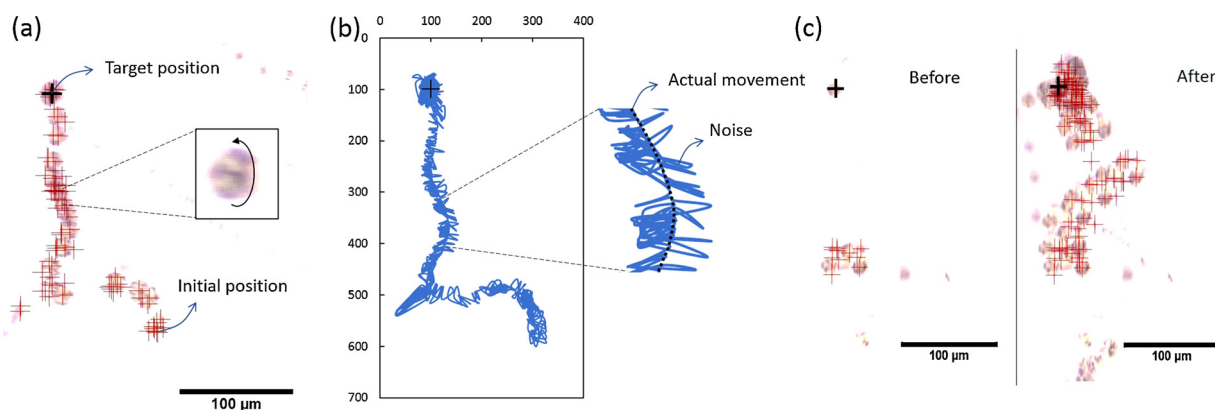


Fig. 7. The closed-loop control of a single and a group of breast cancer cells. (a) The stacked images of a single MCF-7 after controlling and its rotation direction. (b) The recorded trajectory of the single cell to target position at (100, 100) pixels. The zoomed image on the right shows actual trajectory along the dash line while the solid lines on two sides are noises. (c) Before and after being controlled of a group of MCF-7 cells to the target position at (100, 100) pixels.

Interesting Group of Acoustofluidics funded by UK Fluids Network (EP/N032861/1).

Appendix A. Supplementary data

Supplementary material related to this article can be found, in the online version, at doi:<https://doi.org/10.1016/j.snb.2020.128143>.

References

- [1] S. Lin, D. Chen, Y. Xie, Single-cell manipulation technology for cancer research, in: D. Cui (Ed.), *Gastric Cancer Prewarning and Early Diagnosis System*, Springer Netherlands, Dordrecht, 2017, pp. 173–194.
- [2] M.K. Alam, et al., Recent advances in microfluidic technology for manipulation and analysis of biological cells (2007–2017), *Anal. Chim. Acta* 1044 (2018) 29–65.
- [3] A. Barani, et al., Microfluidic integrated acoustic waving for manipulation of cells and molecules, *Biosens. Bioelectron.* 85 (2016) 714–725.
- [4] Pudasaini, S., et al., Continuous flow microfluidic cell inactivation with use of insulating micropillars for multiple electroporation zones. *ELECTROPHORESIS*. 0(ja).
- [5] D. Ahmed, et al., Rotational manipulation of single cells and organisms using acoustic waves, *Nat. Commun.* 7 (2016) 11085.
- [6] K.H. Lam, et al., Multifunctional single beam acoustic tweezer for non-invasive cell/organism manipulation and tissue imaging, *Sci. Rep.* 6 (2016) 37554.
- [7] J.R. Heath, A. Ribas, P.S. Mischel, Single-cell analysis tools for drug discovery and development, *Nat. Rev. Drug Discov.* 15 (2015) 204.
- [8] S. Ishii, K. Tago, K. Senoo, Single-cell analysis and isolation for microbiology and biotechnology: methods and applications, *Appl. Microbiol. Biotechnol.* 86 (5) (2010) 1281–1292.
- [9] S. Lindström, H. Andersson-Svahn, Overview of single-cell analyses: microdevices and applications, *Lab Chip* 10 (24) (2010) 3363–3372.
- [10] M. Wu, et al., Isolation of exosomes from whole blood by integrating acoustics and microfluidics, *Proc. Natl. Acad. Sci.* (2017).
- [11] Z.J. Gartner, C.R. Bertozzi, Programmed assembly of 3-dimensional microtissues with defined cellular connectivity, *Proc. Natl. Acad. Sci.* 106 (12) (2009) 4606–4610.
- [12] G.M. Whitesides, B. Grzybowski, Self-assembly at all scales, *Science* 295 (5564) (2002) 2418–2421.
- [13] P.B. Armstrong, Cell sorting out: the self-assembly of tissues in vitro, *Crit. Rev. Biochem. Mol. Biol.* 24 (2) (1989) 119–149.
- [14] M. Kirschner, T. Mitchison, Beyond self-assembly: from microtubules to morphogenesis, *Cell* 45 (3) (1986) 329–342.
- [15] Y. Du, et al., Directed assembly of cell-laden microgels for fabrication of 3D tissue constructs, *Proc. Natl. Acad. Sci.* 105 (28) (2008) 9522–9527.
- [16] P.Y. Chiou, A.T. Ohta, M.C. Wu, Massively parallel manipulation of single cells and microparticles using optical images, *Nature* 436 (7049) (2005) 370–372.
- [17] A. Ashkin, Optical trapping and manipulation of neutral particles using lasers, *Proc. Natl. Acad. Sci.* 94 (10) (1997) 4853–4860.
- [18] F. Guo, et al., Three-dimensional manipulation of single cells using surface acoustic waves, *Proc. Natl. Acad. Sci.* 113 (6) (2016) 1522–1527.
- [19] X. Ding, et al., Surface acoustic wave microfluidics, *Lab Chip* 13 (18) (2013) 3626–3649.
- [20] S.-C.S. Lin, X. Mao, T.J. Huang, Surface acoustic wave (SAW) acoustophoresis: now and beyond, *Lab Chip* 12 (16) (2012) 2766–2770.
- [21] A. Ozelik, et al., Acoustic tweezers for the life sciences, *Nat. Methods* 15 (12) (2018) 1021–1028.
- [22] L.Y. Yeo, J.R. Friend, Surface acoustic wave microfluidics, *Annu. Rev. Fluid Mech.* 46 (1) (2014) 379–406.
- [23] X. Ding, et al., On-chip manipulation of single microparticles, cells, and organisms using surface acoustic waves, *Proc. Natl. Acad. Sci.* 109 (28) (2012) 11105–11109.
- [24] J. Shi, et al., Acoustic tweezers: patterning cells and microparticles using standing surface acoustic waves (SSAW), *Lab Chip* 9 (20) (2009) 2890–2895.
- [25] C.D. Wood, et al., Formation and manipulation of two-dimensional arrays of micron-scale particles in microfluidic systems by surface acoustic waves, *Appl. Phys. Lett.* 94 (5) (2009) 054101.
- [26] G.D. Skotis, et al., Dynamic acoustic field activated cell separation (DAFACS), *Lab Chip* 15 (3) (2015) 802–810.
- [27] M. Antfolk, et al., Focusing of sub-micrometer particles and bacteria enabled by two-dimensional acoustophoresis, *Lab Chip* 14 (15) (2014) 2791–2799.
- [28] J. Shi, et al., Focusing microparticles in a microfluidic channel with standing surface acoustic waves (SSAW), *Lab Chip* 8 (2) (2008) 221–223.
- [29] J. Shi, et al., Three-dimensional continuous particle focusing in a microfluidic channel via standing surface acoustic waves (SSAW), *Lab Chip* 11 (14) (2011) 2319–2324.
- [30] S.P. Zhang, et al., Digital acoustofluidics enables contactless and programmable liquid handling, *Nat. Commun.* 9 (1) (2018) 2928.
- [31] M.C. Jo, R. Guldiken, Particle manipulation by phase-shifting of surface acoustic waves, *Sens. Actuators A Phys.* 207 (2014) 39–42.
- [32] T. Laurell, F. Petersson, A. Nilsson, Chip integrated strategies for acoustic separation and manipulation of cells and particles, *Chem. Soc. Rev.* 36 (3) (2007) 492–506.
- [33] J. Shi, et al., Continuous particle separation in a microfluidic channel via standing surface acoustic waves (SSAW), *Lab Chip* 9 (23) (2009) 3354–3359.
- [34] Y. Ai, C.K. Sanders, B.L. Marrone, Separation of *Escherichia coli* Bacteria from peripheral blood mononuclear cells using standing surface acoustic waves, *Anal. Chem.* 85 (19) (2013) 9126–9134.
- [35] Y. Chen, et al., High-throughput acoustic separation of platelets from whole blood, *Lab Chip* 16 (18) (2016) 3466–3472.
- [36] G. Destgeer, et al., Continuous separation of particles in a PDMS microfluidic channel via travelling surface acoustic waves (TSAW), *Lab Chip* 13 (21) (2013) 4210–4216.
- [37] C. Devendran, I. Gralinski, A. Neild, Separation of particles using acoustic streaming and radiation forces in an open microfluidic channel, *Microfluid. Nanofluidics* 17 (5) (2014) 879–890.
- [38] P. Li, et al., Acoustic separation of circulating tumor cells, *Proc. Natl. Acad. Sci.* 112 (16) (2015) 4970–4975.
- [39] J. Nam, Y. Lee, S. Shin, Size-dependent microparticles separation through standing surface acoustic waves, *Microfluid. Nanofluidics* 11 (3) (2011) 317–326.
- [40] J. Nam, et al., Density-dependent separation of encapsulated cells in a microfluidic channel by using a standing surface acoustic wave, *Biomicrofluidics* 6 (2) (2012) 024120.
- [41] J. Nam, et al., Separation of platelets from whole blood using standing surface acoustic waves in a microchannel, *Lab Chip* 11 (19) (2011) 3361–3364.
- [42] H. Tsutsui, C.-M. Ho, Cell separation by non-inertial force fields in microfluidic systems, *Mech. Res. Commun.* 36 (1) (2009) 92–103.
- [43] Y. Chen, et al., Rare cell isolation and analysis in microfluidics, *Lab Chip* 14 (4) (2014) 626–645.
- [44] X. Ding, et al., Tunable patterning of microparticles and cells using standing surface acoustic waves, *Lab Chip* 12 (14) (2012) 2491–2497.
- [45] T.D. Nguyen, et al., Patterning and manipulating microparticles into a three-dimensional matrix using standing surface acoustic waves, *Appl. Phys. Lett.* 112 (21) (2018) 213507.
- [46] T. Zheng, et al., Patterning microparticles into a two-dimensional pattern using one column standing surface acoustic waves, *Sens. Actuators A Phys.* 284 (2018) 168–171.
- [47] G.M. Whitesides, The origins and the future of microfluidics, *Nature* 442 (7101) (2006) 368–373.
- [48] I. Bernard, et al., Controlled rotation and translation of spherical particles or living cells by Surface Acoustic Waves, *Lab Chip* (2017).
- [49] B. Kang, et al., High-resolution acoustophoretic 3D cell patterning to construct functional collateral cylindroids for ischemia therapy, *Nat. Commun.* 9 (1) (2018) 5402.
- [50] X. Ding, et al., Standing surface acoustic wave (SSAW) based multichannel cell sorting, *Lab Chip* 12 (21) (2012) 4228–4231.
- [51] J.P. Lata, et al., Surface acoustic waves grant superior spatial control of cells embedded in hydrogel fibers, *Adv. Mater.* 28 (39) (2016) 8632–8638.
- [52] M.N. Shahid, et al., Surface acoustic waves induced micropatterning of cells in gelatin methacryloyl (GelMA) hydrogels, *Biofabrication* 9 (1) (2017) 015020.
- [53] D.J. Collins, et al., Two-dimensional single-cell patterning with one cell per well driven by surface acoustic waves, *Nat. Commun.* 6 (2015) 8686.
- [54] X. Tao, et al., 3D patterning/manipulating microparticles and yeast cells using ZnO/Si thin film surface acoustic waves, *Sens. Actuators B Chem.* 299 (2019) 126991.
- [55] D.F. Crawford, C.A. Smith, G. Whyte, Image-based closed-loop feedback for highly mono-dispersed microdroplet production, *Sci. Rep.* 7 (1) (2017) 10545.
- [56] E. Miller, M. Rotea, J.P. Rothstein, Microfluidic device incorporating closed loop feedback control for uniform and tunable production of micro-droplets, *Lab Chip* 10 (10) (2010) 1293–1301.
- [57] R. Rimsa, et al., A planar surface acoustic wave micropump for closed-loop microfluidics, *Appl. Phys. Lett.* 111 (23) (2017) 234102.
- [58] L.R. Soenksen, et al., Closed-loop feedback control for microfluidic systems through automated capacitive fluid height sensing, *Lab Chip* 18 (6) (2018) 902–914.
- [59] Z. Wang, J. Zhe, Recent advances in particle and droplet manipulation for lab-on-a-chip devices based on surface acoustic waves, *Lab Chip* 11 (7) (2011) 1280–1285.
- [60] S.S. Sadhal, *Acoustofluidics 13: analysis of acoustic streaming by perturbation methods*, *Lab Chip* 12 (13) (2012) 2292–2300.
- [61] L.P. Gor'kov, On the forces acting on a small particle in an acoustical field in an ideal fluid, *Soviet Physics Doklady* 6 (1962) 773–775.
- [62] N. Nama, et al., Numerical study of acoustophoretic motion of particles in a PDMS microchannel driven by surface acoustic waves, *Lab Chip* 15 (12) (2015) 2700–2709.
- [63] M. Hill, N.R. Harris, Ultrasonic particle manipulation, in: S. Hardt, F. Schönfeld (Eds.), *Microfluidic Technologies for Miniaturized Analysis Systems*, Springer US: Boston, MA, 2007, pp. 357–392.
- [64] L. Meng, et al., Precise and programmable manipulation of microbubbles by two-dimensional standing surface acoustic waves, *Appl. Phys. Lett.* 100 (17) (2012) 173701.
- [65] A.K.S. Kumar, et al., High-frequency surface acoustic wave device based on thin-film piezoelectric interdigital transducers, *Appl. Phys. Lett.* 85 (10) (2004) 1757–1759.
- [66] F. Guo, et al., Controlling cell–cell interactions using surface acoustic waves, *Proc. Natl. Acad. Sci.* 112 (1) (2015) 43–48.
- [67] T. Zheng, et al., The role of electric field in microfluidic heating induced by standing surface acoustic waves, *Appl. Phys. Lett.* 112 (23) (2018) 233702.
- [68] H. Bruus, *Acoustofluidics 7: the acoustic radiation force on small particles*, *Lab Chip* 12 (6) (2012) 1014–1021.
- [69] K. Wang, et al., Sorting of tumour cells in a microfluidic device by multi-stage surface acoustic waves, *Sens. Actuators B Chem.* 258 (2018) 1174–1183.
- [70] H. Gomi, M. Kawato, Neural network control for a closed-loop System using Feedback-error-learning, *Neural Netw.* 6 (7) (1993) 933–946.
- [71] P.R. Rogers, J.R. Friend, L.Y. Yeo, Exploitation of surface acoustic waves to drive

size-dependent microparticle concentration within a droplet, *Lab Chip* 10 (21) (2010) 2979–2985.

- [72] S. Li, et al., Standing surface acoustic wave based cell coculture, *Anal. Chem.* 86 (19) (2014) 9853–9859.
- [73] L. Meng, et al., Transportation of single cell and microbubbles by phase-shift introduced to standing leaky surface acoustic waves, *Biomicrofluidics* 5 (4) (2011) 044104.

Tan Dai Nguyen received his B.Eng. degree from the Faculty of Mechanical Engineering, Ho Chi Minh University of Technology, Vietnam in 2016. He is currently pursuing his PhD study since August 2016 under the supervision of Prof. Du Hejun in the School of Mechanical and Aerospace Engineering, Nanyang Technological University, Singapore. His research interests include surface acoustic waves, microfluidics, cells manipulation.

Richard (YongQing) Fu is a professor in University of Northumbria at Newcastle, UK. He obtained his PhD degree from Nanyang Technological University, Singapore, and then worked as a Research Fellow in Singapore-Massachusetts Institute of Technology Alliance, and a Research Associate in University of Cambridge. He was a lecturer in Heriot-Watt University, Edinburgh, UK, and then a reader in Thin Film Centre in University of West of Scotland, Glasgow, UK, before, moving to Newcastle, UK. He has extensive experience in smart thin film/materials, biomedical microdevices, lab-on-a-chip, microelectromechanics, MEMS, nanotechnology, sensors and microfluidics. He published over 360 science citation index (SCI) journal papers and his current SCI H-index is 45 with over 8500 citations.

Van-Thai Tran received his B.E. in mechanical engineering from the Ho Chi Minh University of Technology, Vietnam in 2014 and his Ph.D. degree from Nanyang Technological University, Singapore in 2019. He had a short period of time working as a

software engineer at Robert Bosch Engineering and Business Solutions Vietnam in 2014. He has been working as a postdoctoral research fellow at Nanyang Technological University since 2019. His research focuses on additive manufacturing and printed functional material.

Sanam Pudasaini received his bachelor's degree (BEng) in Mechanical Engineering from Kathmandu University, Nepal in 2014. He is currently pursuing his Ph.D. under the supervision of Prof. Yang Chun, Charles and Dr. Ng Sum Huan, Gary at the School of Mechanical and Aerospace Engineering, NTU. His research interests include electro-poration-based inactivation of microorganisms, microfluidics and electrokinetics for cell manipulation.

Archana Gautam received her B.E. in biomedical engineering from Purbanchal University, Nepal in 2014 and her Ph.D. degree from Materials Science and Engineering department of Nanyang Technological University, Singapore in 2019. She is currently working as a postdoctoral research fellow under Assistant Professor Huang Changjin in Mechanical and Aerospace Engineering department of Nanyang Technological University. Her research interests include nano-bio interaction, nano-toxicity, drug delivery, tissue engineering.

Hejun Du is currently an associate professor in the School of Mechanical and Aerospace Engineering, Nanyang Technological University, Singapore. He obtained both B.E. and M.E. from the Nanjing University of Aeronautics and Astronautics, China, and his PhD from Imperial College, UK. His research interests include (1) numerical and computational methods for engineering applications; (2) MEMS and microfluidics; (3) smart materials and their engineering applications. He has published over 200 international refereed journal papers, more than 100 conference papers and a few invited book chapters. His journal papers were cited over 4000 times in the SCI with a H-index of 36.